




Quantum phase detection generalization from marginal quantum neural network modelsSaverio Monaco ^{1,2,*}, Oriël Kiss ^{1,3,*}, Antonio Mandarino ^{4,†}, Sofia Vallecorsa ¹ and Michele Grossi ^{1,‡}¹European Organization for Nuclear Research (CERN), Geneva 1211, Switzerland²Department of Physics, University of Padova, 35122 Padova PD, Italy³Department of Particle and Nuclear Physics, University of Geneva, Geneva 1211, Switzerland⁴International Centre for Theory of Quantum Technologies, University of Gdańsk, Jana Bażyńskiego 1A, 80-309 Gdańsk, Poland

(Received 18 August 2022; revised 9 December 2022; accepted 17 January 2023; published 10 February 2023)

Quantum machine learning offers a promising advantage in extracting information about quantum states, e.g., phase diagram. However, access to training labels is a major bottleneck for any supervised approach, preventing getting insights about new physics. In this Letter, using quantum convolutional neural networks, we overcome this limit by determining the phase diagram of a model where analytical solutions are lacking, by training only on marginal points of the phase diagram, where integrable models are represented. More specifically, we consider the axial next-nearest-neighbor Ising Hamiltonian, which possesses a ferromagnetic, paramagnetic, and antiphase, showing that the whole phase diagram can be reproduced.

DOI: [10.1103/PhysRevB.107.L081105](https://doi.org/10.1103/PhysRevB.107.L081105)

Introduction. Quantum machine learning (QML) [1], where parametrized quantum circuits [2] act as statistical models, has attracted much attention recently, with applications to natural sciences [3–8] or in generative modeling [9–13]. Even if QML models benefit from high expressivity [14] and demonstrated superiority over classical models in some specific cases [15,16], it is still unclear what kind of advantage could be obtained with quantum computers [17] in the era of deep neural networks.

Quantum data, on the other hand, could be a natural paradigm to apply QML, where quantum advantages have already been demonstrated [18]. There is hope that quantum data could be collected via quantum sensors [19], and eventually directly linked to quantum computers. In this Letter, we emulate the possibility of working with quantum data by constructing them directly on a quantum device. We use a variational ground state solver to obtain approximations of the true ground states in order to mimic noisy real world data. Specifically, this Letter addresses the computation of the phase diagram of the ground states of a Hamiltonian H using a supervised learning approach. Even if similar problems have already been explored for the binary case [20,21], with multiple classes [22] and computed on a superconducting platform [23], all of these approaches suffer from a limitation by construction, a bottleneck. In fact, since labels are needed for the training, and because they are computed analytically or numerically, these techniques can only speed up

calculations, but cannot extend beyond their validated domain. Alternatively, anomaly detection (AD), an unsupervised learning technique, has been proposed [24,25] as a way to bypass this bottleneck, by finding structure inside the data set. However, AD can only obtain qualitative, possibly unstable, results and the performance can therefore be difficult to assess. Instead, the proposed approach provides a clear prediction for the boundaries of the adopted model, with the possibility to evaluate the performance on a validation set.

This Letter numerically demonstrates that QML can make predictions to regions where analytical labels do not exist, after being only trained on easily computable subregions. Moreover, QML only needs very few training labels to do so, as already pointed out by [26]. In particular, we make a step toward an out-of-distribution generalization [28], where the training and testing set do not belong to the same data distribution, which is known to be a difficult task [29]. This drastically changes the perspective, extending QML capabilities to extrapolate and eventually discover new physics when trained on well-established simpler models.

The model. We consider the axial next-nearest-neighbor Ising (ANNNI) model

$$H = J \sum_{i=1}^N \sigma_x^i \sigma_x^{i+1} - \kappa \sigma_x^i \sigma_x^{i+2} + h \sigma_z^i, \quad (1)$$

where σ_a^i are the Pauli matrices acting on the i th spin, $a \in \{x, y, z\}$, and we assume open boundary conditions. The energy scale of the Hamiltonian is given by the coupling constant J (without loss of generality we set $J = 1$), while the dimensionless parameters κ and h account for the next-nearest-neighbor interaction and the transverse magnetic field, respectively. We restrict ourselves to $\kappa \geq 0$, $h \geq 0$, and even N . The difference of sign between the nearest and next-nearest interactions, leading to a ferro- or antiferromagnetic exchange in the system, is responsible for the magnetic frustration. Thence, the ANNNI model offers the possibility to study

*These authors contributed equally to this work.

†antonio.mandarino@ug.edu.pl

‡michele.grossi@cern.ch

the competing mechanism of quantum fluctuations due to the transverse magnetic field and frustration. The phase diagram of the quantum model at $T = 0$ K temperature has been studied mainly by renormalization group or Monte Carlo techniques in d dimensions exploiting also the correspondence with the classical analog in $d + 1$ dimensions [30–35]. The phase diagram is quite rich and three phases have been confirmed, separated by two second-order phase transitions. The first, for low frustration ($\kappa < 0.5$) of the Ising type, separates the ferromagnetic and the paramagnetic phases along the line $h_I(\kappa) \approx \frac{1-\kappa}{\kappa} (1 - \sqrt{\frac{1-3\kappa+4\kappa^2}{1-\kappa}})$. The other one, of a commensurate-incommensurate type, appears between the paramagnetic phase and an antiphase for values of the field $h_C(\kappa) \approx 1.05\sqrt{(\kappa - 0.5)(\kappa - 0.1)}$, in the high frustration sector ($\kappa > 0.5$). As usual, the paramagnetic phase is the disordered one, in contrast with the two ordered phases: the ferromagnetic and the antiphase one. In particular, they are different because the former is characterized by all the spins aligned along the field direction, and the latter has a four-spin periodicity, composed of repetitions of two pairs of spins pointing in opposite directions. The point $\kappa = 0.5$ represents a multicritical point. We mention here that other relevant lines have been numerically addressed but not confirmed: one signaling an infinite-order phase transition of the Berezinskii-Kosterlitz-Thouless (BKT) type for $h_{\text{BKT}}(\kappa) \approx 1.05(\kappa - 0.5)$, delimiting a floating phase between the paramagnetic and the antiphase [34], and a disorder line where the model is exactly solvable, known as the Peschel-Emery (PE) line $h_{\text{PE}}(\kappa) \approx \frac{1}{4\kappa} - \kappa$ [33,36].

Variational state preparation. The purpose of the variational quantum eigensolver (VQE) [37] is to calculate the ground state energy of a Hamiltonian $H(\kappa, h)$ on a quantum computer. Using the Rayleigh-Ritz variational principle, the VQE minimizes the energy expectation value of a parametrized wave function and has been successfully applied in quantum chemistry [38–40], in nuclear physics [41–43], or in frustrated magnetic systems [44,45]. Here, we are interested in the final eigenstates, represented by an ansatz $|\psi(\theta; \kappa, h)\rangle$, to be used as quantum data. Typically, the ansatz is chosen as a hardware-efficient (HEA) quantum circuit [38,46], which is built with low connectivity and gates that can be easily run on noisy intermediate-scale quantum (NISQ) [47] devices. For instance, we use $D = 6(9)$ repetitions of a layer consisting of free rotations around the y axis $R_y(\theta) = e^{-i\theta\sigma_y/2}$ and controlled-NOT (CNOT) gates with linear connectivity $\text{CX}_{i,i+1}$ for $0 \leq i < N$ [48], for $N = 6(12)$ spin systems. The optimization is performed using the gradient-descent-based ADAM algorithm [49], with an initial learning rate of 0.3 and a parameter recycling scheme to improve the convergence [50]. Moreover, we note that the VQE can also be used to recursively compute excited states [51], which we used to show that the ground states of the ANNNI model are only degenerate at the boundaries in the phase diagram, where the ground states corresponding to the different phases are competing, excluding the bit flip symmetry at $h = 0$. Finally, we assess the accuracy of the VQE states by comparing with the exact energy and observe that the relative error ratio is always below 1%. Moreover, it seems that the energy accuracy distribution is able to reveal the Peschel-

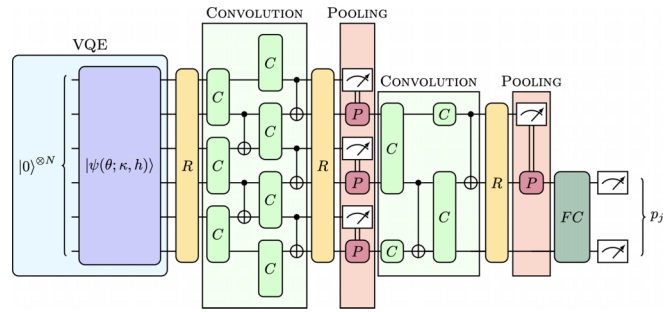


FIG. 1. Circuit architecture: VQE states (blue) are the input of the quantum convolutional neural network composed of free rotations R (yellow), convolutions C (light green), pooling P (red), and a fully connected layer F (dark green).

Emery line, since the predicted energy values are more accurate along it. More details about the implementation, optimization, degeneracy, and accuracy can be found in the Supplemental Material [52].

Quantum convolutional neural networks (QCNNs). QCNNs are a class of quantum circuits, inspired by classical convolutional neural networks (CNNs) [53], originally proposed in Ref. [20]. The QCNN is trained to detect quantum phase transitions, effectively learning an observable $O(\theta)$ that linearly separates two states $|\psi_A\rangle$ and $|\psi_B\rangle$ from two different phases A and B , such that $\langle \psi_A | O(\theta) | \psi_A \rangle < 0 < \langle \psi_B | O(\theta) | \psi_B \rangle$ [54], which exist since the phases in the ANNNI model are not topological. Intuitively, nontopological phases of matter exhibit macroscopic differences, which can be captured by the variational observable $O(\theta)$. In principle, quantum phase detection could be performed by measuring different string order parameters (SOPs) [20]. However, the SOP vanishes near the phase transition, thus requiring exponentially many samples for the classification. On the other hand, the QCNN output is much sharper, therefore reducing the sample complexity. This changes quantum phase detection to the task of designing and training an appropriate ansatz.

In our implementation, the QCNN starts with a free rotation layer around the y axis, followed by blocks consisting of convolutions, free rotations, and pooling layers that halve the number of qubits to k until $k = \lceil \log_2(K) \rceil$, where K is the total number of quantum phases. Finally, a fully connected layer and measurement are performed in the computational basis. An example with $N = 6$ qubits is shown in Fig. 1 where we have free y -axis rotations (yellow), $R(\vec{\theta}) = \bigotimes_{i=1}^N R_y(\vec{\theta}_i)$, two-qubit convolutions (light green) $C(\theta) = \bigotimes_{i=1}^2 R_y(\theta)$, pooling (red) $P(\vec{\theta}, \phi, b) = R_y(\vec{\theta}_b)R_x(\phi)$ with $b \in \{0, 1\}$ the value of the measured qubit, and a two-qubit fully connected (dark green) gate $F(\vec{\theta}^{(1)}, \vec{\theta}^{(2)}) = [\bigotimes_{i=1}^2 R_y(\vec{\theta}_1^{(i)})R_x(\vec{\theta}_2^{(i)})R_y(\vec{\theta}_3^{(i)})]\text{CX}_{1,2}$.

QCNNs have been shown to be resistant to barren plateaus [55] due to their distance from low $T2$ design and are therefore good candidates for any quantum learning tasks. The analogy with CNN holds in the quantum settings since convolution and pooling layers are functions of shared parameters and the reduction of the circuit's dimension is guaranteed by the intermediate measurement. The whole algorithm flow starts with the QCNN taking as input ground

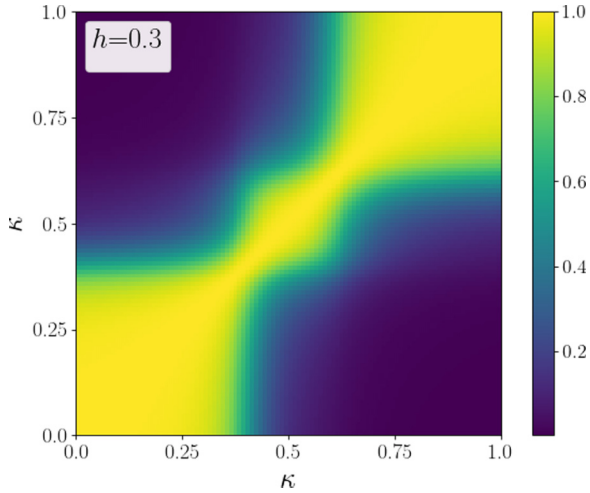


FIG. 2. Fidelity between the ground states of the ANNNI model at $h = 0.3$ and $N = 12$. We observe three different clusters, corresponding to the ferromagnetic, paramagnetic, and antiphase, respectively.

states $|\psi(\theta; \kappa, h)\rangle$ from the Hamiltonian family $H(\kappa, h)$, obtained through the VQE. The quantum network then outputs the probability $p_j(\kappa, h)$ of being in one of the $K = 3$ phases (ferromagnetic, paramagnetic, or antiphase), where $p_j(\kappa, h)$ is computed as the probability of measuring the state $|01\rangle, |10\rangle, |11\rangle$ on the two output qubits. Since the phase diagram of the ANNNI model only contains three phases, the state $|00\rangle$ is interpreted as a *garbage* class.

Generalization. The main contribution of this Letter is to demonstrate the ability of QCNN to work in a partial supervised approach and thus get closer to an out-of-distribution generalization by training on a set of easily available labels. We first argue that this generalization is expected to hold according to Ref. [27] if the ground states of the ANNNI model are clustered, i.e., if the fidelity between states in the same phase is high [56–58], while being low between different phases. This is indeed the case as shown in Fig. 2 along the line $h = 0.3$ for the $N = 12$ spin case. Even if the requirements of the generalization results from Ref. [26] do not hold since the training data are only located on the boundaries, and specifically not independent and identically distributed (i.i.d.), we observe a numerical agreement with the generalization error’s scaling behavior predicted in Ref. [26], i.e., $\mathcal{O}(\sqrt{T/n})$, where T is the number of parameters and n the number of training points. Since the QCNN is composed of $T = \mathcal{O}[\log(N)]$ parameters [20], we can control the expected risk by training on $n = \mathcal{O}[\log(N)]$ points.

Training set. The training data set consists of the composition of points from two analytical models derived from the simplification of the physical model used. Specifically, we consider the integrable Ising model in a transverse field in the case $\kappa = 0$ and the *quasiclassical* model when $h = 0$, where quantum fluctuations no longer exist. We demonstrate that QCNNs extend their prediction to the all phase diagram when only trained on the marginal model given by $\mathcal{S}_X^n \subseteq \{(\kappa, h) \in \{0\} \times [0, 2]\} \cup \{(\kappa, h) \in [0, 1] \times \{0\}\}$. We consider three types of subsets $X \in \{GC, G2, U\}$, \mathcal{S}_{GC}^n where n training points are sampled normally around

each critical point $\{(0, 1), (0.5, 0)\}$, \mathcal{S}_{G2}^n where n training points are sampled normally at the middle of each phase $\{(0, 1.5), (0, 0.5), (0.25, 0), (0.75, 0)\}$, and \mathcal{S}_U^n where n data points are drawn uniformly on both axes. The QCNN is trained using the cross entropy \mathcal{L} loss,

$$\mathcal{L} = -\frac{1}{|\mathcal{S}_X^n|} \sum_{(\kappa, h) \in \mathcal{S}_X^n} \sum_{j=1}^K y_j(\kappa, h) \log [p_j(\kappa, h)], \quad (2)$$

between the one-hot classical labels $y_j(\kappa, h)$ and the predictions on the training region \mathcal{S}_X^n of the phase space.

Results. Once we have introduced the problem and defined the techniques used, we can analyze the quality of the results obtained under ideal conditions with a quantum simulator.

We study our ability to reconstruct the phase diagram of the ANNNI model, characterized by a nontrivial disordered paramagnetic phase, the ordered ferromagnetic phase, and the antiphase one. To test the stability of the proposed approach, we consider the model with an increasing number of spins $N = 6, 12$ and sampling a different number of points $0 < n \leq 100$ used for the training. By virtue of the quality of the results, we evaluated the influence of different sampling of the training points corresponding to the two physical models that could affect the quality of the classification. A summary of the results can be qualitatively seen in Fig. 3, while more quantitative results for the QCNN are displayed in the Supplemental Material [52]. In the first row, we have the phase diagram reconstruction for the ANNNI model with six spins, where the black lines represent the analytical transition explained above in the model section. The second line in the figure shows the same for a system with $N = 12$ spins.

The first column shows the accuracy, computed on the whole phase space, as a function of the number of training points n , for the Gaussian centered around the critical points $X = GC$ (blue), around the middle of each phase $X = G2$ (black), and the uniform $X = U$ (red) sampling scheme, where the error bars correspond to one standard deviation from ten independent runs. We observe that the accuracy quickly increases with n , before saturating for $n \geq 20$, as argued in Ref. [26], and that the sampling strategy does not play a major role. More importantly, sampling away from the critical points is enough. The second column displays the phase diagram obtained with the QCNN trained on $n = 40$ points. Color shades represent the continuous probability distribution of the QCNN for our multiclass classifier as a probability mixture (blue, green, and yellow times the relevant probability), while the red lines represent the predicted boundaries. The individual probabilities of each phases predicted by the QCNN are shown in the Supplemental Material [52]. The last column instead shows the comparison to the unsupervised learning approach inspired from Ref. [25] where the autoencoder is trained to compress the single red cross $|\psi\rangle$, and tested on the remaining points. In a nutshell, the autoencoder is expected to perform poorly if the states are far away in the Hilbert space, i.e., if they belong to different phases, thus leading to a high compression score. The color scale shows the compression loss of each state. Additional details about the implementation of the anomaly detection can be found in the Supplemental Material [52]. It is worth noting that although only one training point is sufficient to

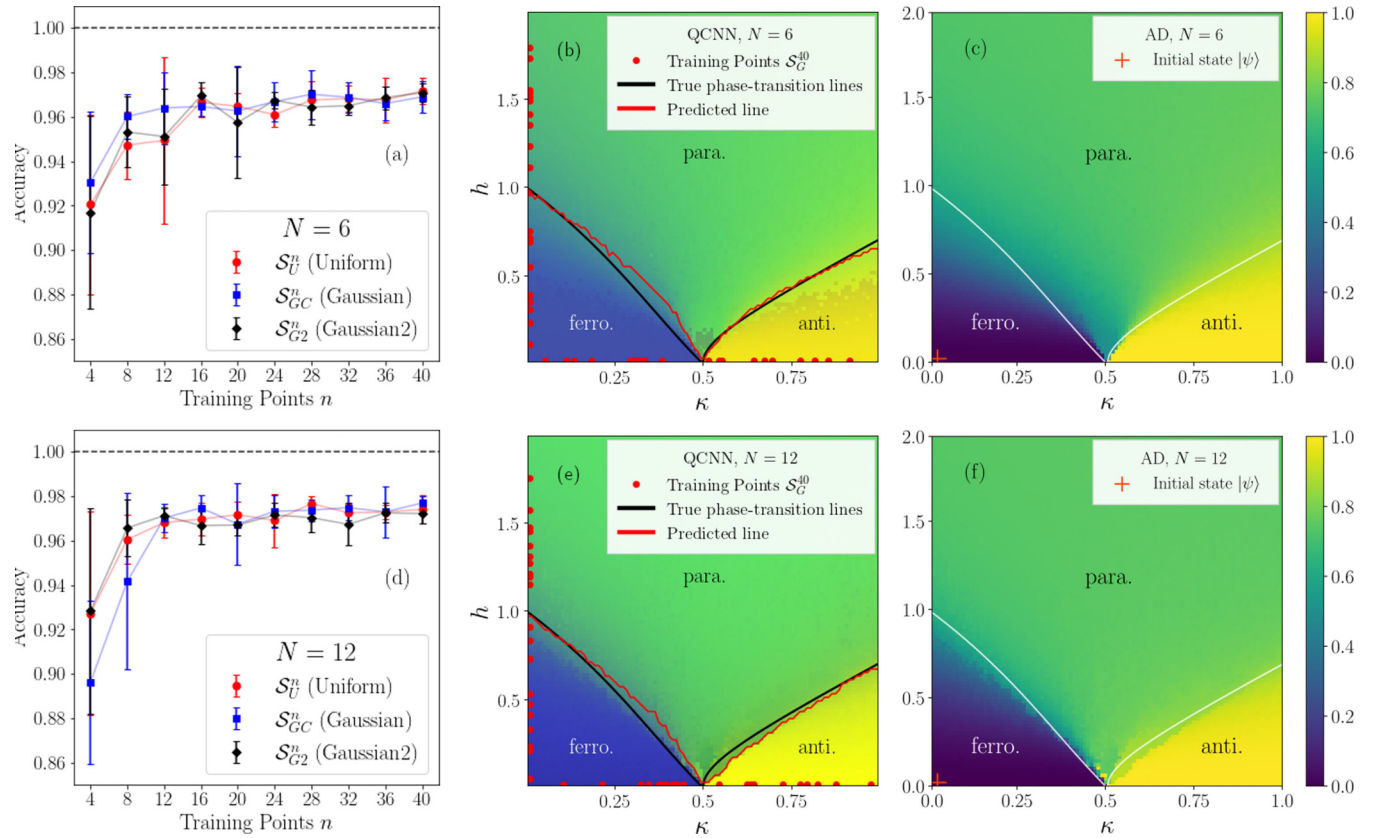


FIG. 3. Quantum phase classification. (a) shows the classification accuracy of the QCNN as a function of the number of training points n , for the Gaussian centered around the critical points (GC blue), Gaussian centered around the middle of each phase ($G2$ black), and uniform sampling (red). (b) displays the phase diagram predicted by the QCNN trained on S_{G2}^{40} (red dots) where the color represents the probability mixture of being in one of the three phases and the red lines the predicted boundaries, while (c) shows the anomaly score for $N = 6$ spin systems trained on the initial state $|\psi\rangle$ (red cross). (d)–(f) are similar but for $N = 12$ spins. The black lines are $h_l(\kappa)$ for $\kappa < 0.5$ and $h_c(\kappa)$ for $\kappa > 0.5$.

obtain a qualitatively good phase diagram, only QCNNS allow a quantitative prediction for the phase. Moreover, while the QCNNS are stable when changing the training set, it is easy to find initial states where AD performs poorly, for instance, by starting in the paramagnetic phase. The relatively good performance of AD can be explained by the product state nature of the training point. Hence, the product state can be easily compressed with the autoencoder, while states corresponding to a high magnetic field cannot.

Conclusions. This Letter addresses the computation of the phase diagram of a nonintegrable model, by training a QCNN on the limiting integrable regions of the considered ANNNI model. We provide numerical evidence that the QCNNS are able to generalize from non-i.i.d. training data, which is a challenging task in general. The numerical simulations suggest that QCNNS can carry this task with more than 97% accuracy, using only $n = 20$ quantum data points distributed on the two integrable axes of the phase space. Moreover, the data points do not need to be close to the critical points. The accuracy of the QCNN quickly increases to reach its maximum as a function of the number of training points, suggesting that QCNNS can generalize from a few data points. Being a supervised method, the QCNN is not able to detect phases that are not present in the training set S_X^n , i.e., the boundaries, such as the BKT phase transition and the PE

line. Nevertheless, AD is also not able to reveal them and is limited to qualitative predictions, while a supervised approach gives quantitative results whose quality can be easily evaluated on the validation set. Moreover, by approaching out-of-distribution generalization, we propose a solution to the bottleneck of needing training labels, that are generally challenging to obtain. Consequently, we make a step into extending the reach of QML to useful applications in physics. Future work should be performed to detect phases not present in the training set, such as the floating phase or the PE line, by either affording $\mathcal{O}(1)$ training points inside these unrepresented phases or mixing the QCNN with the unsupervised approach.

The code used to generate the data set and the figures of the present Letter is publicly available [59].

Acknowledgments. The authors would like to thank Zoë Holmes for useful discussions about generalization. S.M., O.K., and M.G. are supported by CERN through the CERN Quantum Technology Initiative. A.M. is supported by Foundation for Polish Science (FNP), IRAP project ICTQT, Contract No. 2018/MAB/5, cofinanced by EU Smart Growth Operational Program, and (Polish) National Science Center (NCN), MINIATURA DEC-2020/04/X/ST2/01794.

- [1] J. Biamonte, P. Wittek, N. Pancotti, P. Rebentrost, N. Wiebe, and S. Lloyd, Quantum machine learning, *Nature (London)* **549**, 195 (2017).
- [2] M. Benedetti, E. Lloyd, S. Sack, and M. Fiorentini, Parameterized quantum circuits as machine learning models, *Quantum Sci. Technol.* **4**, 043001 (2019).
- [3] O. Kiss, F. Tacchino, S. Vallecorsa, and I. Tavernelli, Quantum neural networks force field generation, *Mach. Learn.: Sci. Technol.* **3**, 035004 (2022).
- [4] V. S. Ngairangbam, M. Spannowsky, and M. Takeuchi, Anomaly detection in high-energy physics using a quantum autoencoder, *Phys. Rev. D* **105**, 095004 (2022).
- [5] C. Zhou, J. Chan, W. Guan, S. Sun, A. Z. Wang, S. L. Wu, M. Livny, F. Carminati, A. Di Meglio, A. C. Y. Li, J. Lykken, P. Spentzouris, S. Y.-C. Chen, S. Yoo, and T.-C. Wei, Application of quantum machine learning to high energy physics analysis at LHC using IBM quantum computer simulators and IBM quantum computer hardware, *PoS* **390**, 930 (2021).
- [6] S. L. Wu, J. Chan, W. Guan, S. Sun, A. Wang, C. Zhou, M. Livny, F. Carminati, A. D. Meglio, A. C. Y. Li, J. Lykken, P. Spentzouris, S. Y.-C. Chen, S. Yoo, and T.-C. Wei, Application of quantum machine learning using the quantum variational classifier method to high energy physics analysis at the LHC on IBM quantum computer simulator and hardware with 10 qubits, *J. Phys. G: Nucl. Part. Phys.* **48**, 125003 (2021).
- [7] Y. Li, R.-G. Zhou, R. Xu, J. Luo, and W. Hu, A quantum deep convolutional neural network for image recognition, *Quantum Sci. Technol.* **5**, 044003 (2020).
- [8] K. Mitarai, M. Negoro, M. Kitagawa, and K. Fujii, Quantum circuit learning, *Phys. Rev. A* **98**, 032309 (2018).
- [9] D. M. Brian Coyle, V. Danos, and E. Kashefi, The Born supremacy: Quantum advantage and training of an Ising Born machine, *npj Quantum Inf.* **6**, 60 (2020).
- [10] C. Zoufal, A. Lucchi, and S. Woerner, Quantum generative adversarial networks for learning and loading random distributions, *npj Quantum Inf.* **5**, 103 (2019).
- [11] M. S. Rudolph, N. B. Toussaint, A. Katarbwa, S. Johri, B. Peropadre, and A. Perdomo-Ortiz, Generation of High-Resolution Handwritten Digits with an Ion-Trap Quantum Computer, *Phys. Rev. X* **12**, 031010 (2022).
- [12] O. Kiss, M. Grossi, E. Kajomovitz, and S. Vallecorsa, Conditional Born machine for Monte Carlo event generation, *Phys. Rev. A* **106**, 022612 (2022).
- [13] A. Delgado and K. E. Hamilton, Unsupervised quantum circuit learning in high energy physics, *Phys. Rev. D* **106**, 096006 (2022).
- [14] A. Abbas, D. Sutter, C. Zoufal, A. Lucchi, A. Figalli, and S. Woerner, The power of quantum neural networks, *Nat. Comput. Sci.* **1**, 403 (2021).
- [15] H.-Y. Huang, M. Broughton, M. Mohseni, R. Babbush, S. Boixo, H. Neven, and J. R. McClean, Power of data in quantum machine learning, *Nat. Commun.* **12**, 2631 (2021).
- [16] J. R. Glick, T. P. Gujarati, A. D. Corcoles, Y. Kim, A. Kandala, J. M. Gambetta, and K. Temme, Covariant quantum kernels for data with group structure, [arXiv:2105.03406](https://arxiv.org/abs/2105.03406).
- [17] M. Schuld and N. Killoran, Is quantum advantage the right goal for quantum machine learning?" *PRX Quantum* **3**, 030101 (2022).
- [18] H.-Y. Huang, M. Broughton, J. Cotler, S. Chen, J. Li, M. Mohseni, H. Neven, R. Babbush, R. Kueng, J. Preskill, and J. R. McClean, Quantum advantage in learning from experiments, *Science* **376**, 1182 (2022).
- [19] C. D. Marciniak, T. Feldker, I. Pogorelov, R. Kaubruegger, D. V. Vasilyev, R. van Bijnen, P. Schindler, P. Zoller, R. Blatt, and T. Monz, Optimal metrology with programmable quantum sensors, *Nature (London)* **603**, 604 (2022).
- [20] I. Cong, S. Choi, and M. D. Lukin, Quantum convolutional neural networks, *Nat. Phys.* **15**, 1273 (2019).
- [21] A. V. Uvarov, A. S. Kardashin, and J. D. Biamonte, Machine learning phase transitions with a quantum processor, *Phys. Rev. A* **102**, 012415 (2020).
- [22] M. Lazzarin, D. E. Galli, and E. Prati, Multi-class quantum classifiers with tensor network circuits for quantum phase recognition, *Phys. Lett. A* **434**, 128056 (2022).
- [23] J. Herrmann, S. M. Llima, A. Remm, P. Zapletal, N. A. McMahon, C. Scarato, F. Swiadek, C. K. Andersen, C. Hellings, S. Krinner, N. Lacroix, S. Lazar, M. Kerschbaum, D. C. Zanuz, G. J. Norris, M. J. Hartmann, A. Wallraff, and C. Eichler, Realizing quantum convolutional neural networks on a superconducting quantum processor to recognize quantum phases, *Nat. Commun.* **13**, 4144 (2022).
- [24] K. Kottmann, P. Huembeli, M. Lewenstein, and A. Acín, Unsupervised Phase Discovery with Deep Anomaly Detection, *Phys. Rev. Lett.* **125**, 170603 (2020).
- [25] K. Kottmann, F. Metz, J. Fraxanet, and N. Baldelli, Variational quantum anomaly detection: Unsupervised mapping of phase diagrams on a physical quantum computer, *Phys. Rev. Res.* **3**, 043184 (2021).
- [26] M. C. Caro, H.-Y. Huang, M. Cerezo, K. Sharma, A. Sornborger, L. Cincio, and P. J. Coles, Generalization in quantum machine learning from few training data, *Nat. Commun.* **13**, 4919 (2022).
- [27] L. Banchi, J. Pereira, and S. Pirandola, Generalization in quantum machine learning: A quantum information standpoint, *PRX Quantum* **2**, 040321 (2021).
- [28] M. C. Caro, H.-Y. Huang, N. Ezzell, J. Gibbs, A. T. Sornborger, L. Cincio, P. J. Coles, and Z. Holmes, Out-of-distribution generalization for learning quantum dynamics, [arXiv:2204.10268](https://arxiv.org/abs/2204.10268).
- [29] H. Ye, C. Xie, T. Cai, R. Li, Z. Li, and L. Wang, Towards a theoretical framework of out-of-distribution generalization, in *Advances in Neural Information Processing Systems*, edited by A. Beygelzimer, Y. Dauphin, P. Liang, and J. W. Vaughan (Neural Information Processing Systems Foundation, San Diego, 2021).
- [30] W. Selke, The ANNNI model — theoretical analysis and experimental application, *Phys. Rep.* **170**, 213 (1988).
- [31] P. R. C. Guimarães, J. A. Plascak, F. C. Sá Barreto, and J. Florencio, Quantum phase transitions in the one-dimensional transverse Ising model with second-neighbor interactions, *Phys. Rev. B* **66**, 064413 (2002).
- [32] A. K. Chandra and S. Dasgupta, Floating phase in the one-dimensional transverse axial next-nearest-neighbor Ising model, *Phys. Rev. E* **75**, 021105 (2007).
- [33] M. Beccaria, M. Campostrini, and A. Feo, Density-matrix renormalization-group study of the disorder line in the quantum axial next-nearest-neighbor Ising model, *Phys. Rev. B* **73**, 052402 (2006).
- [34] M. Beccaria, M. Campostrini, and A. Feo, Evidence for a floating phase of the transverse ANNNI model at high frustration, *Phys. Rev. B* **76**, 094410 (2007).

- [35] A. Canabarro, F. F. Fanchini, A. L. Malvezzi, R. Pereira, and R. Chaves, Unveiling phase transitions with machine learning, *Phys. Rev. B* **100**, 045129 (2019).
- [36] I. Peschel and V. Emery, Calculation of spin correlations in two-dimensional Ising systems from one-dimensional kinetic models, *Z. Phys. B* **43**, 241 (1981).
- [37] A. Peruzzo, J. McClean, P. Shadbolt, M.-H. Yung, X.-Q. Zhou, P. J. Love, A. Aspuru-Guzik, and J. L. O'Brien, A variational eigenvalue solver on a photonic quantum processor, *Nat. Commun.* **5**, 4213 (2014).
- [38] A. Kandala, A. Mezzacapo, K. Temme, M. Takita, M. Brink, J. M. Chow, and J. M. Gambetta, Hardware-efficient variational quantum eigensolver for small molecules and quantum magnets, *Nature (London)* **549**, 242 (2017).
- [39] P. K. Barkoutsos, J. F. Gonthier, I. Sokolov, N. Moll, G. Salis, A. Fuhrer, M. Ganzhorn, D. J. Egger, M. Troyer, A. Mezzacapo, S. Filipp, and I. Tavernelli, Quantum algorithms for electronic structure calculations: Particle-hole hamiltonian and optimized wave-function expansions, *Phys. Rev. A* **98**, 022322 (2018).
- [40] J. Romero, R. Babbush, J. R. McClean, C. Hempel, P. J. Love, and A. Aspuru-Guzik, Strategies for quantum computing molecular energies using the unitary coupled cluster ansatz, *Quantum Sci. Technol.* **4**, 014008 (2019).
- [41] E. F. Dumitrescu, A. J. McCaskey, G. Hagen, G. R. Jansen, T. D. Morris, T. Papenbrock, R. C. Pooser, D. J. Dean, and P. Lougovski, Cloud Quantum Computing of an Atomic Nucleus, *Phys. Rev. Lett.* **120**, 210501 (2018).
- [42] I. Stetcu, A. Baroni, and J. Carlson, Variational approaches to constructing the many-body nuclear ground state for quantum computing, *Phys. Rev. C* **105**, 064308 (2022).
- [43] O. Kiss, M. Grossi, P. Lougovski, F. Sanchez, S. Vallecorsa, and T. Papenbrock, Quantum computing of the ${}^6\text{Li}$ nucleus via ordered unitary coupled clusters, *Phys. Rev. C* **106**, 034325 (2022).
- [44] A. Uvarov, J. D. Biamonte, and D. Yudin, Variational quantum eigensolver for frustrated quantum systems, *Phys. Rev. B* **102**, 075104 (2020).
- [45] M. Grossi, O. Kiss, F. De Luca, C. Zollo, I. Gremese, and A. Mandarino, Finite-size criticality in fully connected spin models on superconducting quantum hardware, *Phys. Rev. E* **107**, 024113 (2023).
- [46] S. Sim, P. D. Johnson, and A. Aspuru-Guzik, Expressibility and entangling capability of parameterized quantum circuits for hybrid quantum-classical algorithms, *Adv. Quantum Technol.* **2**, 1900070 (2019).
- [47] J. Preskill, Quantum computing in the NISQ era and beyond, *Quantum* **2**, 79 (2018).
- [48] M. A. Nielsen and I. L. Chuang, *Quantum Computation and Quantum Information: 10th Anniversary Edition* (Cambridge University Press, Cambridge, UK, 2010).
- [49] D. P. Kingma and J. Ba, ADAM: A method for stochastic optimization, in *3rd International Conference on Learning Representations, ICLR 2015, San Diego, CA, USA, May 7–9, 2015, Conference Track Proceedings*, edited by Y. Bengio and Y. LeCun (ICLR, 2015).
- [50] S. M. Harwood, D. Trenev, S. T. Stober, P. Barkoutsos, T. P. Gujarati, S. Mostame, and D. Greenberg, Improving the variational quantum eigensolver using variational adiabatic quantum computing, *ACM Trans. Quantum Comput.* **3**, 1 (2022).
- [51] O. Higgott, D. Wang, and S. Brierley, Variational quantum computation of excited states, *Quantum* **3**, 156 (2019).
- [52] See Supplemental Material at <http://link.aps.org/supplemental/10.1103/PhysRevB.107.L081105> for details about the construction and accuracy of the variational quantum data set, the individual probabilities outputted by the supervised quantum convolutional neural network, and a complete description of the anomaly detection procedure.
- [53] Y. LeCun, B. Boser, J. S. Denker, D. Henderson, R. E. Howard, W. Hubbard, and L. D. Jackel, Backpropagation applied to handwritten zip code recognition, *Neural Comput.* **1**, 541 (1989).
- [54] H.-Y. Huang, R. Kueng, G. Torlai, V. V. Albert, and J. Preskill, Provably efficient machine learning for quantum many-body problems, *Science* **377**, eabk3333 (2022).
- [55] A. Pesah, M. Cerezo, S. Wang, T. Volkoff, A. T. Sornborger, and P. J. Coles, Absence of Barren Plateaus in Quantum Convolutional Neural Networks, *Phys. Rev. X* **11**, 041011 (2021).
- [56] M. Bina, A. Mandarino, S. Olivares, and M. G. A. Paris, Drawbacks of the use of fidelity to assess quantum resources, *Phys. Rev. A* **89**, 012305 (2014).
- [57] A. Mandarino, M. Bina, S. Olivares, and M. G. Paris, About the use of fidelity in continuous variable systems, *Int. J. Quantum Inf.* **12**, 1461015 (2014).
- [58] A. Mandarino, M. Bina, C. Porto, S. Cialdi, S. Olivares, and M. G. A. Paris, Assessing the significance of fidelity as a figure of merit in quantum state reconstruction of discrete and continuous-variable systems, *Phys. Rev. A* **93**, 062118 (2016).
- [59] <https://cern-qpd-annni.readthedocs.io/en/latest/>.